ACCOUNTS of chemical research

Article

pubs.acs.org/accounts

Seeding a New Kind of Garden: Synthesis of Architecturally Defined Multimetallic Nanostructures by Seed-Mediated Co-Reduction

Rebecca G. Weiner, Meredith R. Kunz, and Sara E. Skrabalak*

Department of Chemistry, Indiana University—Bloomington, 800 East Kirkwood Ave., Bloomington, Indiana 47405, United States

CONSPECTUS: Bimetallic nanoparticles display unique optical and catalytic properties that depend on crystallite size and shape, composition, and overall architecture. They may serve as multifunctional platforms as well. Unfortunately, many routes toward shape and architecturally controlled bimetallic nanocrystals yield polydisperse samples on account of the challenges associated with homogeneously nucleating a defined bimetallic phase by co-reduction methods. Developed by the Skrabalak laboratory, seed-mediated co-reduction (SMCR) involves the simultaneous co-reduction of two metal precursors to deposit metal onto shape-controlled metal nanocrystalline seeds. The central premise is that seeds will serve as preferential and structurally defined platforms for bimetallic deposition, where the shape of the seeds can be transferred to the shells. With Au−Pd as a model system, a set of design principles has been established for the bottom-up synthesis of shape-controlled bimetallic nanocrystals by SMCR. This strategy is successful at synthesizing symmetrically stellated Au−Pd nanocrystals with a variety of symmetries and core@shell Au@Au−Pd nanocrystals. Achieving nanocrystals with high morphological control via SMCR is governed by the following parameters: seed size, shape, and composition as well as the kinetics of seeded growth (through manipulation of synthetic parameters such as pH and metal precursor ratios). For example, larger seeds yield larger nanocrystals as does increasing the amount of metal deposited relative to the number of seeds. This increase in nanocrystal size leads to red-shifts in their localized surface plasmon resonance. Additionally, seed shape directs the overgrowth process during SMCR so the resultant nanocrystals adopt related symmetries. The ability to tune structure is important due to the size-, shape- and composition-dependent optical properties of bimetallic nanocrystals. Using this toolkit, the light scattering and absorption properties of Au−Pd octopods, 8-branched nanocrystals, could be tuned and were shown to be highly sensitive to changes in refractive index. The refractive index sensitivity displayed a linear correlation to the localized surface plasmon resonance initial position, where the sensitivity is greater than that of monometallic Au structures. Due to their bimetallic composition and unique architecture enabled by SMCR, Au−Pd octopods are promising refractive index based sensors. This Account summarizes the underlying principles for synthesis of bimetallic nanocrystals by SMCR, which have been established by systematic manipulation of synthetic parameters in a model Au−Pd system. These principles are anticipated to be general to other bimetallic systems, allowing for the design and synthesis of new nanocrystals with fascinating optical and catalytic properties.

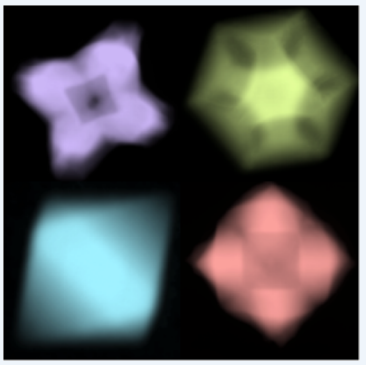

1. INTRODUCTION

Noble metal nanoparticles (NPs) are of interest because of their unique properties that arise from particle size, shape, composition, and architecture.[1] Bimetallic NPs similarly are of interest and can display composition-dependent multifunctionality through adjustment of the metallic distribution.[2−5] For example, core@shell Au@Pd nanoplates can be refractive index (RI) sensors to monitor hydrogen adsorption.[6] Moreover, Wang et al. deposited Pd islands on the tips of Au nanorods to facilitate Suzuki coupling via plasmonic catalysis and photothermal heating.[7] Similar structures have served as catalysts for a variety of reactions, where the Au component enables reaction monitoring by surface-enhanced Raman spectroscopy (SERS).[8,9]

Given the potential use of bimetallic nanomaterials,[3,5,10−13] a critical need for synthetic routes to structurally well-defined bimetallic nanocrystals (NCs) exists. Seed-mediated methods are premier routes toward well-defined NPs,[14−16] as exemplified with the synthesis of Au nanorods from quasi-spherical Au seeds.[17] With seeded methods, preformed NPs serve as a preferential platform for deposition of additional material, where primary (i.e., homogeneous) nucleation is separated from growth.[1] This feature is exploited in seed-mediated co-reduction (SMCR, Scheme 1), a method developed by the Skrabalak group, to overcome the challenge of homogeneously nucleating defined bimetallic phases.[18] Compared to traditional seeded methods where one metal is deposited, SMCR involves the reduction of two metal precursors simultaneously to deposit bimetallic shells, with the central hypothesis being that the shape of seeds could be transferred to the bimetallic shells.[19]

SMCR was originally demonstrated for the synthesis of Au−Pd NCs as a model system, with Au and Pd precursors being reduced to deposit metal onto shape-controlled Au seeds. This system was selected because of the good lattice match between Au and Pd (~96%), the resistance of Au seeds to galvanic replacement, and the ability to reduce Au and Pd precursors under similar conditions.[19] Moreover, there were many examples demonstrating Au@Pd NC formation.[11,20,21] These observations

Received: June 17, 2015
Published: September 4, 2015

DOI: 10.1021/acs.accounts.5b00300
Acc. Chem. Res. 2015, 48, 2688−2695

Scheme 1. Comparison of Seed-Mediated Co-Reduction with a Traditional Seeded Method

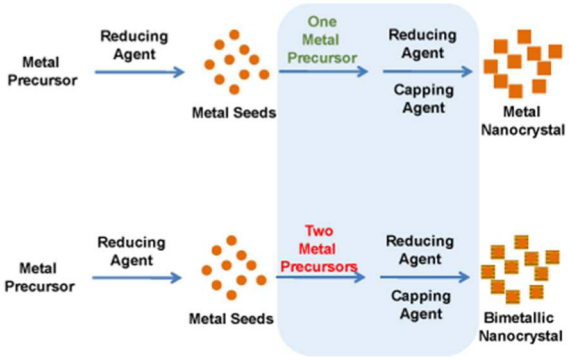

suggested that Au−Pd deposition onto seeds should be possible, with seed shape being transferred to the shells. Indeed, deposition of Au−Pd shells onto octahedral Au seeds yielded octahedral NCs with alloyed Au−Pd shells (Figure 1).[19] SMCR also provides a route to symmetrically stellated Au−Pd NCs, originally as octopods, eight-branched NCs with O_h symmetry (Figure 1).[19] The conditions that account for convex and concave Au−Pd NCs by SMCR are discussed in section 2. Interestingly, the symmetry of stellation and nanostructure architecture (i.e., hollow versus solid) can be manipulated by changing seed shape and composition, respectively (section 3).[22,23] This control provides a means to tune the optical properties of Au−Pd NCs, with Au−Pd octopods serving as a model system to investigate the emergence of RI sensitivity in a bimetallic system (section 4). Collectively, these experiments provide design strategies toward bimetallic NCs with defined architectures (section 5).

2. CO-REDUCTION AND STRUCTURE CONTROL

In the first demonstration of SMCR, Au and Pd precursors were simultaneously reduced in water with L-ascorbic acid (L-aa) (room temperature) in the presence of cetyltrimethylammonium bromide (CTAB) and octahedral Au seeds.[19] The seeds adopted a cubic intermediate during growth to facilitate Au−Pd octopod formation, where eight branches proceed along ⟨111⟩ directions, each from a cube vertex.[23] Scanning transmission electron microscopy (STEM) coupled with energy dispersive X-ray spectroscopy (EDX) confirmed that the NC interiors are predominantly Au, and Pd is localized on surfaces and at NC tips (Figure 1, row 5).[19] Thus, experiments were designed to study how synthetic conditions affected morphology of Au−Pd NCs and kinetics of NC growth.

First, the Au:Pd precursor ratio during SMCR was varied.[18] Scanning electron microscopy (SEM) images of products show that increasing the Pd precursor concentration relative to Au precursor led to an increase in particle size and the tips of the octopodal NCs became flattened. STEM-EDX mapping shows that the {111}-terminated tips are predominantly Pd. The reaction pH was also varied.[18] Again, octopod tips became shorter and flattened, with octahedral NCs forming at the lowest pH (Figure 1). Significantly, the selected seed shape was transferred to the final NCs.

Morphological changes were attributed originally to changes in the growth kinetics because of pH-dependent reducing capability of L-aa. Specifically, as the reducing capability of L-aa decreases, thermodynamically favored structures (i.e., convex NCs) would be anticipated on account of slower metal deposition rates.[24] However, this analysis relied heavily on qualitative comparisons to observations made by other groups regarding branched NC formation.[1,25] Recently, a quantitative analysis of this system was undertaken where Au and Pd deposition rates were measured as a function of pH. The amounts of Au and Pd at different reaction points were measured by inductively coupled plasma mass spectrometry (ICP-MS).

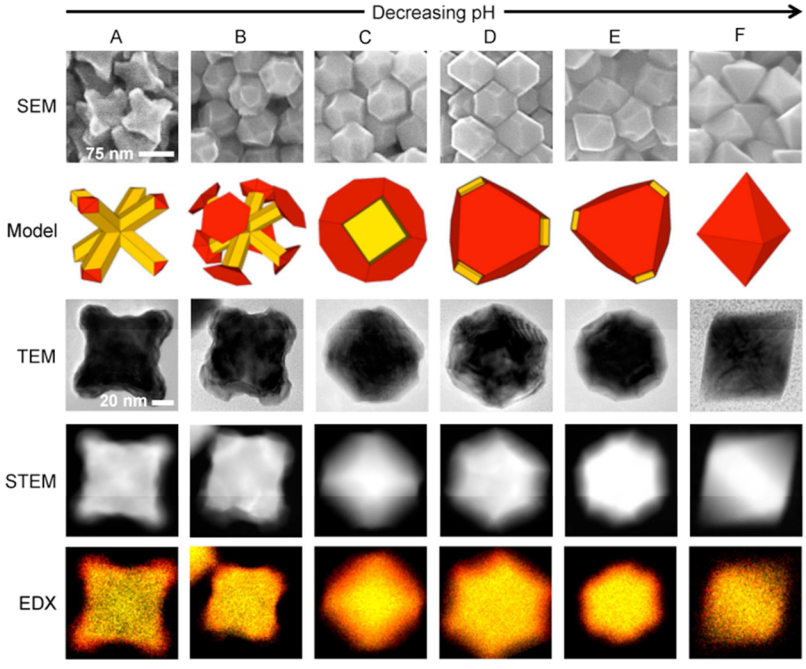

Figure 1. Top to bottom: SEM, 3-D model, TEM, STEM, and elemental mapping, where Au is represented by yellow and Pd by red of Au−Pd NCs synthesized at decreasing pH. Adapted with permission from ref 18. Copyright 2012 American Chemical Society.

DOI: 10.1021/acs.accounts.5b00300
Acc. Chem. Res. 2015, 48, 2688−2695

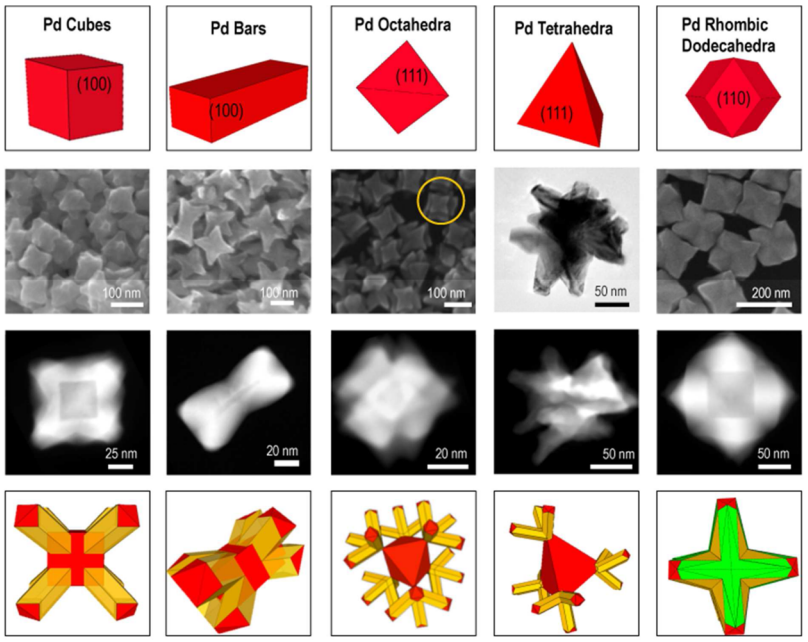

Figure 2. Top to bottom: 3-D model of Pd seeds and SEM (except Pd tetrahedra, TEM), STEM and 3-D models of branched NCs where Au is represented by yellow and Pd by red. Left to right: Pd cubes and corresponding octopods, Pd bars and corresponding nanobowties, Pd octahedra and corresponding 24-branched NCs, Pd tetrahedra and corresponding 12-branched NCs, and Pd rhombic dodecahedra and corresponding octopods. Adapted with permission from refs 34 and 23. Copyright 2013 and 2014, respectively, American Chemical Society.

These measurements found no clear dependence with pH at a constant Au:Pd precursor ratio despite dramatic changes in morphology.[24] Alternative interpretations include that the HCl used to manipulate pH may also facilitate oxidative etching of Pd during deposition or that the structure of the CTAB bilayer is modified.[26] At this point, the origin of morphology development as a function of pH remains unclear.

Additionally, changes in morphology were observed with changes in the ion content of the synthesis. In the original Au–Pd octopod synthesis, CTAB was used in high concentration, yielding branched structures with slightly blunted tips. Replacing CTAB with equimolar cetyltrimethylammonium chloride (CTAC), octopodal structures with sharper tips formed.[18,24] Adding KBr to the CTAC system yielded octopods with blunted tips. Interestingly, higher concentrations of KBr led to expression of {111} facets and the formation of hopper-like Au–Pd NCs (i.e., octahemioctahedra). This expression was surprising as {100}-encased metal NCs are common when bromide is present.[1] This deviation was attributed to a decreased rate of Pd deposition compared to Au on account of $[CTA]_2PdBr_4$ complex formation, that is, a kinetic effect.[1] The association of Pd^{2+} and Br^- was corroborated by UV–visible spectroscopy, with the kinetic effect verified by measuring the amount of metal deposited at different reaction points by ICP-MS.[18] Thus, the addition of Br^- to this system provides a means to tune Au–Pd NCs between hopper-like structures and symmetrically branched octopods.

This comprehensive study of how different synthetic parameters influence the bimetallic architecture during SMCR of Au–Pd NCs reveals that small changes in conditions can induce large morphological changes. This finding is not unlike syntheses to monometallic NCs. However, the necessity for two metal precursors for bimetallic NC formation can complicate analyses of morphology development.[19] Still, these results indicate that trends in monometallic systems can serve as a starting place when designing routes to new bimetallic structures.[15,27]

3. SEED SHAPE AND COMPOSITION IN STRUCTURE CONTROL

Seeded methods have been used to synthesize a variety of core@shell structures, where the seeds template shell deposition.[28−30] The final structures often adopt the shape of the seeds, and the same strategies used to manipulate shape in homogeneously nucleated systems can be applied to seeded syntheses. For example, Habas et al. synthesized conformal Pt@Pd NCs by depositing Pd onto cubic Pt seeds.[15] NO, generated in situ, was used as a capping agent to synthesize cuboctahedral and octahedral Pt@Pd NCs; otherwise, cubic Pt@Pd NCs formed. Yet other parameters unique to seeded systems also can influence morphology.

For example, seeded methods may be used to produce branched structures, where the seeds direct the branching. In fact, Maksimuk et al. synthesized Pt multipods with 0–4 branches from a central seed, where the number of branches correlated with the specific seed structure.[27] Habas et al. also found that the degree of lattice mismatch between the seed and overgrowth material contributes to morphology development. For example, a small lattice mismatch between the seed and depositing metal facilitates conformal core@shell NC formation, exemplified by the Pt@Pd system (0.77% mismatch).[31,32] With a larger lattice mismatch, anisotropic growth can be induced. This tendency is exemplified by deposition of Au onto cubic Pt seeds (4.02% mismatch), where Au nanorods half embedded in Pt cubes result.[15] Finally, Fan et al. studied the impact of bond energy difference between seeds and depositing metals and found that this parameter could account for island versus layer-by-layer growth.[28] Thus, bond and surface energy along with lattice mismatch are likely intertwined in seeded NC syntheses.

DOI: 10.1021/acs.accounts.5b00300
Acc. Chem. Res. 2015, 48, 2688−2695

In the SMCR synthesis of Au−Pd NCs, we hypothesized that the symmetry of the Au seeds accounted for the symmetry of the structures achieved in Figure 1, and that by changing the symmetry of the seeds, NCs with different symmetries—including different patterns of stellation—should be possible. Moreover, we were curious why eight-branched NCs formed from octahedral seeds, as this observation suggested that branch growth initiates at seed faces rather than vertices.[19] Kinetically controlled syntheses typically facilitate deposition preferentially at undercoordinated sites.[1] Unfortunately, understanding the symmetry relationships between the Au seeds and final NCs is challenging as Au deposits primarily first in this system.[18] This situation makes elucidating the Au seed metal from the Au-rich overgrowth difficult. However, selecting Pd seeds provides a compositional boundary in this system, effectively serving as "TEM-labels" analogous to fluorophores in confocal microscopy to mark specific features.[33,34] From elemental mapping, the symmetry relationships between shape-controlled seeds and concave NCs then could be established.[23,34]

For example, SMCR of Au and Pd precursors with single-crystalline Pd seeds resulted in branched growth from each vertex.[34] When {100}-terminated Pd nanocubes are used as seeds, eight-branched NCs result, with one branch growing from each vertex of the cube (Figure 2, column 1). The O_h symmetry of the cubes is conserved in the final branched NCs. The cubic seed is evident in the STEM image. Electron diffraction (ED) confirmed that branched growth occurred in ⟨111⟩ directions. The use of {100}-terminated Pd nanobars as seeds yielded similar results (Figure 2, column 2).[34] One branch grew from each vertex of the nanobar for a total of eight branches, with the D_{4h} symmetry of the seed conserved in the resultant nanobowties. However, changing the seed shape to {111}-terminated octahedra yielded a different result. Instead of one branch growing from each vertex, four branches grew from each of the six vertices, for a total of 24 branches (Figure 2, column 3).[34] For a given vertex, each branch grows in a different [111] direction and the O_h symmetry of the seeds is conserved. Likewise, {111}-terminated tetrahedral Pd seeds yielded structures with more branches than seed vertices (Figure 2, column 4). In this case, three branches grew from each of the four vertices of the tetrahedra in energetically equivalent ⟨111⟩ directions for a total of 12 branches. Finally, SMCR of Au and Pd precursors with Pd rhombic dodecahedral seeds with 14 vertices resulted in eight-branched NCs (Figure 2, column 5).[23] This finding may seem surprising given the results obtained with {100}- and {111}-terminated structures; however, this structure is accounted for by considering crystal symmetry. Rhombic dodecahedra are {110}-terminated structures and have eight vertices along ⟨111⟩ directions (like the vertices of a cube; denoted as V_{111} herein) and six vertices along ⟨100⟩ directions (like the vertices of an octahedron; denoted as V_{100} herein). Considering the preference for branched growth in {111} directions, one branch can grow from each V_{111} for a total of eight branches; this result is similar to that obtained from cubic Pd seeds and account for the octopodal structure. Four branches can grow from each V_{100}; however, these branches would be along the edges of the Pd seeds (denoted in green in 3-D model). This consideration accounts for the thickness at the base of the protruding branches. In all cases, branches are primarily Au, with Pd localized at surfaces and branch tips. This composition is represented in the models shown in Figure 2.[23,34]

Stellated structures are likewise obtained with single-crystalline Au seeds; however, as a first approximation, the relationship between seed vertices and branched growth does not hold. For example, Au octahedra yield eight-branched octopods with O_h symmetry rather than 24-branched NCs. Upon further study, a cubic intermediate was isolated before branch formation, which supports correlation between vertices and branches.[23] A cubic intermediate does not form with octahedral Pd seeds. The formation of cubic Au intermediates from single-crystalline Au seeds is attributed to faster diffusion of Au adatoms on Au seeds than on Pd seeds.[23] Thus, when {111}-terminated Au octahedra or {110}-terminated Au rhombic dodecahedra are used as seeds, {100}-terminated cubic Au intermediates account for octopods, similar to those obtained with either Au or Pd cubes (Figure 3).[23]

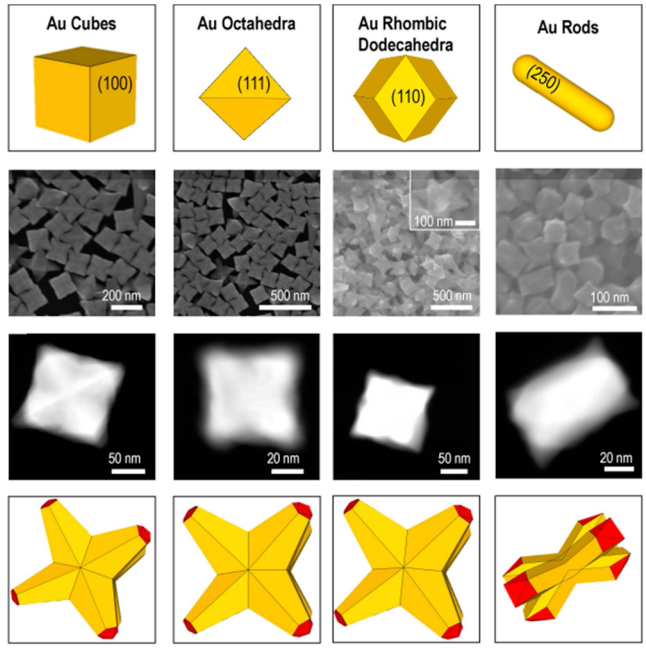

Figure 3. Top to bottom: 3-D model of Au seeds and SEM, STEM, and 3-D models of branched NCs. Au is represented by yellow and Pd by red. Left to right: Au cubes and corresponding octopods, Au octahedra and corresponding octopods, Au rhombic dodecahedra and corresponding octopods, and Au rods and corresponding nanobowties. Adapted with permission from ref 23. Copyright 2014 American Chemical Society.

When {250}-terminated Au nanorods were used as seeds, 8-branched NCs formed, similar to the bowties from Pd nanobars (Figure 3, column 4).[8] Like the Pd seeds, branches grow in ⟨111⟩ directions and are composed of Au, with Pd at surfaces and branch tips.[23]

The introduction of twin planes in Pd or Au seeds accesses additional branching patterns. For example, when Pd right bipyramids were used as seeds for co-reduction of Au and Pd precursors, five-branched pentapods result.[34] Right bipyramids have five vertices and are {100}-terminated with a (111) twin plane through the center of the particle (Figure 4, row 1). Upon SMCR, one branch grows from each vertex. However, unlike the aforementioned results with single-crystalline seeds, ED indicates that the three branches growing from the twin plane proceed along ⟨112⟩ directions, with the twin plane conserved though each branch. The two axial branches grow in ⟨111⟩ directions, and the D_{3h} symmetry of the right bipyramidal seed is conserved.[34] When {711}-terminated Au pentatwinned bipyramids with D_{5h} symmetry are used as seeds, nanostructures with two to three branches per bipyramid end are produced (Figure 4,

DOI: 10.1021/acs.accounts.5b00300
Acc. Chem. Res. 2015, 48, 2688−2695

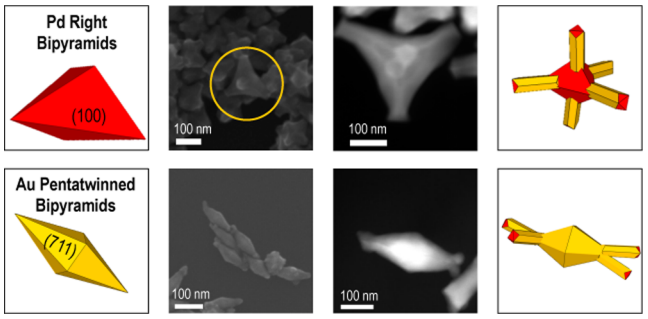

Figure 4. Top row: 3-D model of Pd right bipyramid seed and SEM, STEM, and 3-D model of corresponding pentapod. Bottom row: Au pentatwinned bipyramid seed and corresponding branched particles. Adapted with permission from refs 34 and 23. Copyright 2013 and 2014, respectively, American Chemical Society.

row 2).[23] Due to the pentatwinned nature of the seed, five branches per bipyramid end were expected. The origin of this deviation is unclear at this time. Branch direction could not be determined by ED due to five overlapping diffraction patterns from the pentatwinned seed, but a back-of-the-envelope calculation approximated branched growth as in ⟨111⟩ directions for C_1 symmetry. Unlike the previously discussed examples with Au NC seeds, symmetry is not conserved between the seeds and resulting NPs. Moreover, the maximum number of branches was not realized.[23] Both studies with twinned Pd and Au seeds display new symmetries and number of branches compared to single-crystalline studies and expand the classes of NCs possible by SMCR.

Remarkably, by changing seed composition to a metal other than Au or Pd, new structures can be synthesized by SMCR, including hollow and trimetallic nanostructures. For example, when Au and Pd precursors were co-reduced with L-aa in the presence of cubic Ag seeds, polycrystalline Ag−Au−Pd NPs with hollow interiors form, as confirmed by STEM-EDX elemental mapping and ED (Figure 5A−D).[22] The hollow structures form

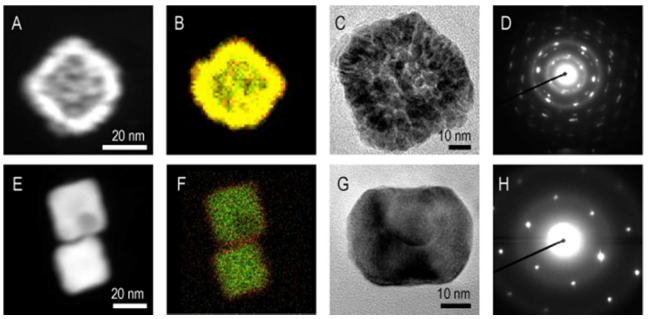

Figure 5. (A) STEM of Ag−Au−Pd hollow nanoparticle. (B) Corresponding EDX elemental mapping where Au is represented by yellow, Pd by red, and Ag by green. (C) TEM. (D) ED of a Ag−Au−Pd hollow particle. (E) STEM of a pair of Ag@Au−Pd trimetallic nanoparticles. (F) Corresponding EDX elemental mapping. (G) TEM. (H) ED of single Ag@Au−Pd particle. Reproduced from ref 22 with permission from The Royal Society of Chemistry.

due to galvanic replacement, a reduction−oxidation process in which one material (here, Ag nanocubes) is oxidized as a sacrificial template as a second material deposits (Pd and Au).[35] As the standard reduction potentials of the depositing metals ($AuCl_4^-$/Au: 1.002 V versus SHE; $PdCl_4^{2-}$/Pd: 0.591 V versus SHE) are greater than that of the seed (AgCl/Ag: 0.2223 V versus SHE), oxidation of Ag templates is anticipated with Au^{3+} and Pd^{2+} under standard conditions.[22] Unlike a traditional galvanic replacement process, a secondary reducing agent is present (L-aa), which reduces the Ag^+ released from the template to deposit Ag onto the surfaces of the nanostructures. This process gives rise to a trimetallic exterior, as revealed by STEM-EDX elemental mapping (Figure 5B).[22] By increasing the reducing strength of L-aa through reaction pH, the final product can be tuned from polycrystalline Ag−Au−Pd NPs to single-crystalline Ag@Au−Pd NCs (Figure 5E−G). This change in architecture arises because Au and Pd deposition is rapid and protects the Ag seeds from galvanic replacement. This example illustrates that by selecting seeds with a composition different from what is being deposited, both new nanoarchitectures and compositions are possible.[22]

By tuning seed composition and structure, NPs with a variety of symmetries, crystallinity, and architectures are possible by SMCR. Au seeds stabilize to {100}-terminated intermediates and yield octopods upon co-reduction of Au and Pd precursors; whereas Pd seeds are stable and allow the synthesis of a variety of symmetrically branched NCs by tuning the number of branches through seed shape. By tuning the seed composition to a material with a lower reduction potential than the metals being deposited, galvanic replacement can tune the final bi- or trimetallic NP in both composition and architecture.

4. OPTICAL PROPERTIES

Work by Xie et al. shows that Au nanostars are promising platforms for SERS due to local electric field enhancement at their sharp tips.[36] Similarly, the stellated Au−Pd nanostructures described provide field enhancement but also can provide new function and enhanced properties on account of their bimetallic composition, as described in the Introduction. Considering the Au/Pd octopods, they display well-defined localized surface plasmon resonances (LSPRs) in the visible to near-IR even with the incorporation of Pd, a poor plasmonic metal. On account of the seeded method, size control is easily achieved by varying the amount of metal deposited relative to the number of seeds. This approach was used to tune the face diagonal of the Au−Pd octopods between 60 and 150 nm while holding the Au:Pd precursor ratio in the overgrowth step constant. The tip width also increases with this approach. UV−visible spectroscopy of the NCs in water reveals one band, which red-shifts from 565 to 746 nm and broadens as the NCs increase in size (Figure 6A).[37] The red-shift is expected as the restoring force of the free electrons decreases with size. The broadening is likely due to variations in particle size and bimetallic distribution as the octopods increase in size.[37]

The Au−Pd octopods were evaluated as potential platforms for LSPR sensing by measuring their sensitivity to small changes in RI.[37] For all samples, an expected red-shift was observed as the RI of surrounding media was increased. The RI sensitivity of the Au−Pd octopods increased linearly with LSPR initial position, with the largest octopods having sensitivities around 500 nm/RIU (Figure 6B).[38] Studies by Liz Marzán reported RI sensitivities between 200 and 350 nm/RIU for Au nanostars.[37,39]

Thus, the bimetallic composition has an impact on the RI sensitivity and Au−Pd octopods are promising RI-based sensors.

The LSPR of structures synthesized by SMCR can be tuned through the interior composition of the particles as well. For example, the cubic Ag@Au−Pd NCs (Figure 5G) display two bands at 431 and 254 nm, which are blue-shifted relative to the stellated Au−Pd NCs.[22] The introduction of a hollow interior

DOI: 10.1021/acs.accounts.5b00300
Acc. Chem. Res. 2015, 48, 2688−2695

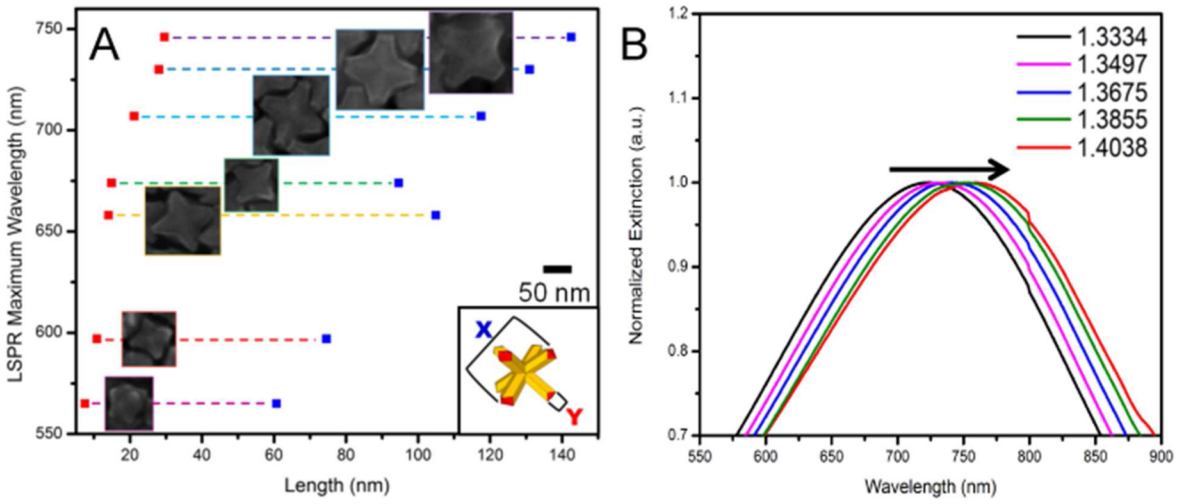

Figure 6. (A) Graph comparing average size along two dimensions (*X* and *Y*, blue and red, respectively) and the LSPR maximum wavelength of Au−Pd octopods shown in representative SEM images. (B) Extinction spectra of largest Au−Pd octopods in various RI, indicated in figure. Adapted with permission from ref 37. Copyright 2012 American Chemical Society.

red-shifts the LSPR. However, these NCs are not stellated, minimizing electric field enhancements. For many applications, stellated structures with far red-shifted LSPRs are desirable.[40] As we found, etching Au−Pd octopods built from cubic Pd seeds with Fe^{3+} can facilitate the selective removal of the Pd interior.[41] By creating a hollow interior within the stellated framework, the LSPR can be shifted past 900 nm. As these examples illustrate, manipulating the interior of nanostructures provides an additional synthetic lever to tune the LSPR.

5. EMERGING DESIGN CRITERIA AND FUTURE OUTLOOK

The culmination of these studies has led to design criteria toward architecturally controlled multimetallic NCs by SMCR.

(1) The final NC size is governed by seed size and amount of depositing metal during SMCR. The use of larger seeds will yield larger NCs. Also, increasing the amount of metal deposited relative to the number of seeds will lead to larger NCs. The ability to tune NC size is important as the position of the LSPR is size-dependent, typically red-shifting with increasing size. This guideline was exemplified by the size-controlled synthesis of Au−Pd octopods, with LSPRs tuned from the visible to near-IR.[37] Similar trends have been observed in traditional seed-mediated syntheses, as originally demonstrated by Natan and co-workers.[1,42]

(2) The final nanoarchitecture (i.e., hollow versus solid; pattern of stellation) is governed by seed surface reactivity during SMCR: (a) Seeds with a lower reduction potential than the overgrowth metals can undergo galvanic replacement to facilitate hollow nanostructure formation during SMCR. Nanostructures with hollow interiors have red-shifted LSPRs. The process of galvanic replacement can be suppressed through the addition of a second reducing agent to form trimetallic NCs. This guideline was exemplified with the use of Ag seeds with Au and Pd codeposition.[22] (b) Diffusion-mediated changes in seed shape can occur during SMCR, ultimately leading to different convex and concave structures.[23] This process was evident with Au deposition on shape-controlled Au seeds, where Au octahedra adopt a cubic Au intermediate before branch formation. In contrast, Pd NCs are stable, with Pd octahedra preserved during SMCR to yield branches from the six vertices of the octahedra.[34]

(3) Under kinetically controlled growth conditions, branch growth will initiate at the vertices of shape-stable seeds.[34] The selection of seeds with different shapes facilitates the synthesis of stellated NCs with different symmetries. The symmetry of the seed is generally conserved in the final NC.[34] In the model Au−Pd system, branch growth proceeds in ⟨111⟩ directions in the absence of twin planes. This relationship between seed shape and stellated NC symmetry is evident with the use of shape-controlled Pd seeds, which can be imaged by STEM-EDX and provide a compositional boundary between the seed metal and Au-rich overgrowth metal.

(4) The kinetics of seeded growth can be manipulated to achieve convex and concave bimetallic NCs by SMCR. This guideline is evident from the pH dependent morphology development in the model Au−Pd NC system, where decreasing the pH facilitates thermodynamically favored convex NC formation rather than stellated NCs.[18,24]

(5) Fine structural features can be tuned through the use of additives in SMCR.[43] This guideline is evident from the study of halides in Au−Pd NC formation by SMCR, where the chloride-to-bromide ratio in the synthesis can be used to tune the sharpness of tips in stellated NCs.[18,43] This phenomenon is also observed in monometallic systems, such as the synthesis of Au nanorods.[44,45]

These guidelines were developed in a Au−Pd model system through systematic manipulation of synthetic parameters coupled with structural analyses of products and measurements of growth kinetics. Given the foundation of these principles in crystal growth and coordination chemistry, they are likely more general then the model Au−Pd system. This claim is supported by research from other groups.

For example, the Qin group demonstrated the synthesis of hollow Ag−Au NCs with enriched Ag by SMCR. Cubic Ag seeds are used, and a Au salt initiates galvanic replacement. Unlike the traditional process, a second reducing agent is present, which co-reduces the released Ag^+ and the Au salt. By adding a large amount of reducing agent, galvanic replacement can be suppressed to produce Ag@Au nanocubes. This example is similar to our recent system where Ag nanocubes are used as seeds for Au and Pd deposition.[46,47] The studies by Qin demonstrate the generality of SMCR toward shape-controlled

DOI: 10.1021/acs.accounts.5b00300
Acc. Chem. Res. 2015, 48, 2688−2695

alloyed NCs. Moreover, the Chen group applied SMCR to achieve compositions challenging to access as shape-defined nanostructures. Cu_xM_{1-x} NCs were synthesized by co-reducing Au, Pt, or Pd salt with a Cu salt to deposit metal onto seeds of the same noble metal.[48] As Cu deposits, alloying and anisotropic growth occurs, facilitating bimetallic nanorod formation. Unlike the Au−Pd model system, alloying with the initial seeds is dominant. This difference likely arises from differences in reaction temperature, with these results highlighting an additional synthetic parameter that can be manipulated to achieve new nanostructures by SMCR.

These studies show the versatility of the SMCR approach. In general, a critical need for synthetic routes to high-quality bimetallic nanostructures exists. However, achieving such structures has been limited because of reliance on co-reduction techniques. As we found, coupling co-reduction with a seeded process provides structurally defined platforms for bimetallic deposition. In turn, a variety of architecturally controlled multimetallic NCs (concave core@shell NCs, symmetrically stellated NCs, shape-controlled alloyed NCs, and hollow nanoarchitectures) can be achieved through simple manipulation of synthetic parameters.

AUTHOR INFORMATION

Corresponding Author

*E-mail: sskrabal@indiana.edu.

Funding

This work was supported by Indiana University start-up funds, NSF Award CHE-1306853, and Research Corporation's Cottrell Scholar Program.

Notes

The authors declare no competing financial interest.

Biographies

Sara E. Skrabalak received a BA in Chemistry from Washington University in St. Louis (2002) and her PhD from the University of Illinois at Urbana - Champaign (2007). She then conducted postdoctoral research at the University of Washington - Seattle with Younan Xia before starting as an Assistant Professor of Chemistry at Indiana University - Bloomington (IU-B, 2008). She is the James Rudy Associate Professor of Chemistry and her group develops new routes to shape-controlled nanomaterials.

Rebecca G. Weiner received her BS in Chemistry at the University of Illinois at Urbana−Champaign where she conducted research with Catherine Murphy. She is a doctoral candidate at IU-B. Her research interests include understanding the growth mechanism of bimetallic nanostructures and electron microscopy.

Meredith R. Kunz received her BS in Chemistry from North Park University in Chicago. She also completed a REU with Teri Odom at Northwestern University. Meredith is a PhD student at IU-B. Her research interests include synthesis of bimetallic nanocrystals by seeded methods and advanced nanostructure characterization.

ACKNOWLEDGMENTS

The authors thank Alison Smith for her feedback. S.E.S. is an Alfred P. Sloan Fellow and Camille Dreyfus Teacher-Scholar.

REFERENCES

(1) Xia, Y.; Xiong, Y.; Lim, B.; Skrabalak, S. E. Shape-Controlled Synthesis of Metal Nanocrystals: Simple Chemistry Meets Complex Physics? *Angew. Chem., Int. Ed.* **2009**, *48*, 60−103.

(2) Marbella, L. E.; Andolina, C. M.; Smith, A. M.; Hartmann, M. J.; Dewar, A. C.; Johnston, K. A.; Daly, O. H.; Millstone, J. E. Gold-Cobalt Nanoparticle Alloys Exhibiting Tunable Compositions, Near-Infrared Emission, and High T2 Relaxivity. *Adv. Funct. Mater.* **2014**, *24*, 6532−6539.

(3) Wang, D.; Li, Y. Bimetallic Nanocrystals: Liquid-Phase Synthesis and Catalytic Applications. *Adv. Mater.* **2011**, *23*, 1044−1060.

(4) DeSantis, C. J.; Weiner, R. G.; Radmilovic, A.; Bower, M. M.; Skrabalak, S. E. Seeding Bimetallic Nanostructures as a New Class of Plasmonic Colloids. *J. Phys. Chem. Lett.* **2013**, *4*, 3072−3082.

(5) Suntivich, J.; Xu, Z.; Carlton, C. E.; Kim, J.; Han, B.; Lee, S. W.; Bonnet, N.; Marzari, N.; Allard, L. F.; Gasteiger, H. A.; Hamad-Schifferli, K.; Shao-Horn, Y. Surface Composition Tuning of Au−Pt Bimetallic Nanoparticles for Enhanced Carbon Monoxide and Methanol Electrooxidation. *J. Am. Chem. Soc.* **2013**, *135*, 7985−7991.

(6) Tang, M. L.; Liu, N.; Dionne, J. A.; Alivisatos, A. P. Observations of Shape-Dependent Hydrogen Uptake Trajectories from Single Nanocrystals. *J. Am. Chem. Soc.* **2011**, *133*, 13220−13223.

(7) Wang, F.; Li, C.; Chen, H.; Jiang, R.; Sun, L.-D.; Li, Q.; Wang, J.; Yu, J. C.; Yan, C.-H. Plasmonic Harvesting of Light Energy for Suzuki Coupling Reactions. *J. Am. Chem. Soc.* **2013**, *135*, 5588−5601.

(8) Huang, J.; Zhu, Y.; Lin, M.; Wang, Q.; Zhao, L.; Yang, Y.; Yao, K. X.; Han, Y. Site-Specific Growth of Au−Pd Alloy Horns on Au Nanorods: A Platform for Highly Sensitive Monitoring of Catalytic Reactions by Surface Enhancement Raman Spectroscopy. *J. Am. Chem. Soc.* **2013**, *135*, 8552−8561.

(9) Heck, K. N.; Janesko, B. G.; Scuseria, G. E.; Halas, N. J.; Wong, M. S. Observing Metal-Catalyzed Chemical Reactions in Situ Using Surface-Enhanced Raman Spectroscopy on Pd−Au Nanoshells. *J. Am. Chem. Soc.* **2008**, *130*, 16592−16600.

(10) Zhou, S.; Jackson, G. S.; Eichhorn, B. AuPt Alloy Nanoparticles for CO-Tolerant Hydrogen Activation: Architectural Effects in Au-Pt Bimetallic Nanocatalysts. *Adv. Funct. Mater.* **2007**, *17*, 3099−3104.

(11) Hong, J. W.; Kim, D.; Lee, Y. W.; Kim, M.; Kang, S. W.; Han, S. W. Atomic-Distribution-Dependent Electrocatalytic Activity of Au−Pd Bimetallic Nanocrystals. *Angew. Chem.* **2011**, *123*, 9038−9042.

(12) Lim, B.; Jiang, M.; Yu, T.; Camargo, P. C.; Xia, Y. Nucleation and Growth Mechanisms for Pd-Pt Bimetallic Nanodendrites and their Electrocatalytic Properties. *Nano Res.* **2010**, *3*, 69−80.

(13) Lim, B.; Jiang, M.; Camargo, P. H. C.; Cho, E. C.; Tao, J.; Lu, X.; Zhu, Y.; Xia, Y. Pd-Pt Bimetallic Nanodendrites with High Activity for Oxygen Reduction. *Science* **2009**, *324*, 1302−1305.

(14) Dovgolevsky, E.; Haick, H. Direct Observation of the Transition Point Between Quasi-Spherical and Cubic Nanoparticles in a Two-Step Seed-Mediated Growth Method. *Small* **2008**, *4*, 2059−2066.

(15) Habas, S. E.; Lee, H.; Radmilovic, V.; Somorjai, G. A.; Yang, P. Shaping Binary Metal Nanocrystals through Epitaxial Seeded Growth. *Nat. Mater.* **2007**, *6*, 692−697.

(16) Laskar, M.; Zhong, X.; Li, Z.-Y.; Skrabalak, S. E. Manipulating the Kinetics of Seeded Growth for Edge-Selective Metal Deposition and the Formation of Concave Au Nanocrystals. *ChemSusChem* **2013**, *6*, 1959−1965.

(17) Murphy, C. J.; Thompson, L. B.; Alkilany, A. M.; Sisco, P. N.; Boulos, S. P.; Sivapalan, S. T.; Yang, J. A.; Chernak, D. J.; Huang, J. The Many Faces of Gold Nanorods. *J. Phys. Chem. Lett.* **2010**, *1*, 2867−2875.

(18) DeSantis, C. J.; Sue, A. C.; Bower, M. M.; Skrabalak, S. E. Seed-Mediated Co-Reduction: A Versatile Route to Architecturally Controlled Bimetallic Nanostructures. *ACS Nano* **2012**, *6*, 2617−2628.

(19) DeSantis, C. J.; Peverly, A. A.; Peters, D. G.; Skrabalak, S. E. Octopods versus Concave Nanocrystals: Control of Morphology by Manipulating the Kinetics of Seeded Growth via Co-Reduction. *Nano Lett.* **2011**, *11*, 2164−2168.

(20) Lee, Y. W.; Kim, M.; Kim, Z. H.; Han, S. W. One-Step Synthesis of Au@Pd Core−Shell Nanooctahedron. *J. Am. Chem. Soc.* **2009**, *131*, 17036−17037.

(21) Lu, C.-L.; Prasad, K. S.; Wu, H.-L.; Ho, J.-a. A.; Huang, M. H. Au Nanocube-Directed Fabrication of Au−Pd Core−Shell Nanocrystals with Tetrahexahedral, Concave Octahedral, and Octahedral Structures

DOI: 10.1021/acs.accounts.5b00300
Acc. Chem. Res. 2015, 48, 2688−2695

and Their Electrocatalytic Activity. *J. Am. Chem. Soc.* **2010**, *132*, 14546−14553.
(22) Weiner, R. G.; Smith, A. F.; Skrabalak, S. E. Synthesis of Hollow and Trimetallic Nanostructures by Seed-Mediated Co-Reduction. *Chem. Commun.* **2015**, *51*, 8872−8875.
(23) Weiner, R. G.; DeSantis, C. J.; Cardoso, M. B. T.; Skrabalak, S. E. Diffusion and Seed Shape: Intertwined Parameters in the Synthesis of Branched Metal Nanostructures. *ACS Nano* **2014**, *8*, 8625−8635.
(24) Bower, M. M.; DeSantis, C. J.; Skrabalak, S. E. A Quantitative Analysis of Anions and pH on the Growth of Bimetallic Nanostructures. *J. Phys. Chem. C* **2014**, *118*, 18762−18770.
(25) Bullen, C.; Zijlstra, P.; Bakker, E.; Gu, M.; Raston, C. Chemical Kinetics of Gold Nanorod Growth in Aqueous CTAB Solutions. *Cryst. Growth Des.* **2011**, *11*, 3375−3380.
(26) Lee, S.; Anderson, L. J. E.; Payne, C. M.; Hafner, J. H. Structural Transition in the Surfactant Layer that Surrounds Gold Nanorods as Observed by Analytical Surface-Enhanced Raman Spectroscopy. *Langmuir* **2011**, *27*, 14748−14756.
(27) Maksimuk, S.; Teng, X.; Yang, H. Roles of Twin Defects in the Formation of Platinum Multipod Nanocrystals. *J. Phys. Chem. C* **2007**, *111*, 14312−14319.
(28) Fan, F.-R.; Liu, D.-Y.; Wu, Y.-F.; Duan, S.; Xie, Z.-X.; Jiang, Z.-Y.; Tian, Z.-Q. Epitaxial Growth of Heterogeneous Metal Nanocrystals: From Gold Nano-octahedra to Palladium and Silver Nanocubes. *J. Am. Chem. Soc.* **2008**, *130*, 6949−6951.
(29) Langille, M. R.; Personick, M. L.; Zhang, J.; Mirkin, C. A. Defining Rules for the Shape Evolution of Gold Nanoparticles. *J. Am. Chem. Soc.* **2012**, *134*, 14542−14554.
(30) Ortiz, N.; Skrabalak, S. E. On the Dual Roles of Ligands in the Synthesis of Colloidal Metal Nanostructures. *Langmuir* **2014**, *30*, 6649−6659.
(31) Peng, Z.; Yang, H. Synthesis and Oxygen Reduction Electrocatalytic Property of Pt-on-Pd Bimetallic Heteronanostructures. *J. Am. Chem. Soc.* **2009**, *131*, 7542−7543.
(32) Lee, H.; Habas, S. E.; Somorjai, G. A.; Yang, P. Localized Pd Overgrowth on Cubic Pt Nanocrystals for Enhanced Electrocatalytic Oxidation of Formic Acid. *J. Am. Chem. Soc.* **2008**, *130*, 5406−5407.
(33) Langille, M. R.; Zhang, J.; Personick, M. L.; Li, S.; Mirkin, C. A. Stepwise Evolution of Spherical Seeds into 20-Fold Twinned Icosahedra. *Science* **2012**, *337*, 954−957.
(34) DeSantis, C. J.; Skrabalak, S. E. Core Values: Elucidating the Role of Seed Structure in the Synthesis of Symmetrically Branched Nanocrystals. *J. Am. Chem. Soc.* **2013**, *135*, 10−13.
(35) Xia, X.; Wang, Y.; Ruditskiy, A.; Xia, Y. 25th Anniversary Article: Galvanic Replacement: A Simple and Versatile Route to Hollow Nanostructures with Tunable and Well-Controlled Properties. *Adv. Mater.* **2013**, *25*, 6313−6333.
(36) Xie, J.; Zhang, Q.; Lee, J. Y.; Wang, D. I. C. The Synthesis of SERS-Active Gold Nanoflower Tags for In Vivo Applications. *ACS Nano* **2008**, *2*, 2473−2480.
(37) DeSantis, C. J.; Skrabalak, S. E. Size-Controlled Synthesis of Au/Pd Octopods with High Refractive Index Sensitivity. *Langmuir* **2012**, *28*, 9055−9062.
(38) Miller, M. M.; Lazarides, A. A. Sensitivity of Metal Nanoparticle Surface Plasmon Resonance to the Dielectric Environment. *J. Phys. Chem. B* **2005**, *109*, 21556−21565.
(39) Barbosa, S.; Agrawal, A.; Rodríguez-Lorenzo, L.; Pastoriza-Santos, I.; Alvarez-Puebla, R. A.; Kornowski, A.; Weller, H.; Liz-Marzán, L. M. Tuning Size and Sensing Properties in Colloidal Gold Nanostars. *Langmuir* **2010**, *26*, 14943−14950.
(40) Zuloaga, J.; Nordlander, P. On the Energy Shift between Near-Field and Far-Field Peak Intensities in Localized Plasmon Systems. *Nano Lett.* **2011**, *11*, 1280−1283.
(41) DeSantis, C. J.; Skrabalak, S. E. Manipulating the Optical Properties of Symmetrically Branched Au/Pd Nanocrystals through Interior Design. *Chem. Commun.* **2014**, *50*, 5367−5369.
(42) Brown, K. R.; Walter, D. G.; Natan, M. J. Seeding of Colloidal Au Nanoparticle Solutions. 2. Improved Control of Particle Size and Shape. *Chem. Mater.* **2000**, *12*, 306−313.
(43) DeSantis, C. J.; Sue, A. C.; Radmilovic, A.; Liu, H.; Losovyj, Y. B.; Skrabalak, S. E. Shaping the Synthesis and Assembly of Symmetrically Stellated Au/Pd Nanocrystals with Aromatic Additives. *Nano Lett.* **2014**, *14*, 4145−4150.
(44) Lohse, S. E.; Burrows, N. D.; Scarabelli, L.; Liz-Marzán, L. M.; Murphy, C. J. Anisotropic Noble Metal Nanocrystal Growth: The Role of Halides. *Chem. Mater.* **2014**, *26*, 34−43.
(45) Ye, X.; Jin, L.; Caglayan, H.; Chen, J.; Xing, G.; Zheng, C.; Doan-Nguyen, V.; Kang, Y.; Engheta, N.; Kagan, C. R.; Murray, C. B. Improved Size-Tunable Synthesis of Monodisperse Gold Nanorods through the Use of Aromatic Additives. *ACS Nano* **2012**, *6*, 2804−2817.
(46) Yang, Y.; Liu, J.; Fu, Z.-W.; Qin, D. Galvanic Replacement-Free Deposition of Au on Ag for Core−Shell Nanocubes with Enhanced Chemical Stability and SERS Activity. *J. Am. Chem. Soc.* **2014**, *136*, 8153−8156.
(47) Yang, Y.; Zhang, Q.; Fu, Z.-W.; Qin, D. Transformation of Ag Nanocubes into Ag−Au Hollow Nanostructures with Enriched Ag Contents to Improve SERS Activity and Chemical Stability. *ACS Appl. Mater. Interfaces* **2014**, *6*, 3750−3757.
(48) Chen, S.; Jenkins, S. V.; Tao, J.; Zhu, Y.; Chen, J. Anisotropic Seeded Growth of Cu−M (M = Au, Pt, or Pd) Bimetallic Nanorods with Tunable Optical and Catalytic Properties. *J. Phys. Chem. C* **2013**, *117*, 8924−8932.

DOI: 10.1021/acs.accounts.5b00300
Acc. Chem. Res. 2015, 48, 2688−2695